一般社団法人　電子情報通信学会
THE INSTITUTE OF ELECTRONICS,
INFORMATION AND COMMUNICATION ENGINEERS

信学技報
IEICE Technical Report
SANE2016-74 (2016-11)

A Study on Maximal Ratio Combining in Stepped Multiple Frequency CPC Radars for Multipath Fading

Manabu AKITA†,　Masato WATANABE†　and　Takayuki INABA†

†Graduate School of Informatics & Engineering, The University of Electro-Communications
1-5-1 Chofugaoka, Chofu, Tokyo, 182-8585 Japan

E-mail: akita.manabu@uec.ac.jp

Abstract Automotive radar plays an important role in such as Autonomous Cruise Control (ACC), Collision Avoidance etc. Multipath fading problem is a technical issue for automotive radar. Non-coherent integration processing, in which the received signal amplitude is averaged, is generally considered to suppress the variance of noise in relatively low signal-to-noise ratio (SNR) situations. Meanwhile coherent integration for signal components (Maximal Ratio Combining (MRC)) is considered to be effective to improve SNR. Authors have been developing stepped multiple frequency Complementary Phase Code (CPC) radar system. The unique radar modulation/demodulation method can achieve a high range resolution and a long-range detection performance by a narrow bandwidth receiver compared to transmitting bandwidth. In this paper, MRC processing candidates for multipath fading in stepped multiple frequency CPC radar operated in 60GHz/76GHz bands are considered. The simulation results comparing to conventional non-coherent integration are also shown.

Key words　Radar, Stepped Multiple Frequency CPC, Multipath fading, Maximal Ratio Combining

1. Introduction

In recent years, radar is expected to be utilized as a part of Intelligent Transport System (ITS). Automotive radar has been generally used in applications such as Autonomous Cruise Control (ACC), Collision Avoidance etc. Our research group has been also developing a self-driving car equipped with radar as shown in Fig.1. Automotive radar generally cannot avoid multipath fading in the environments where the received signal is attenuated by multipath waves reflected on the road surface [1]. The received signal power from the targets such as human and vehicles is possible to be weakened by the multipath waves at the range where the path difference between the direct wave and the multipath wave is odd multiple of half of transmitting wave length. At these ranges, radar cannot detect those targets even in its covering range. For overcoming the multipath fading problem, an antenna mounting method in which the antennas are mounted at different altitude (spatial diversity) can be considered [2]. One is installed on the front bumper and the other is installed on the roof of the vehicle for instance.

However, the mounting method described above is difficult to be adopted from the point of view of the cost and practicality for automotive radar. On the other hand, authors are considering utilizing frequency diversity effect for the multipath fading problem [3]. The frequency bands that can be used for automotive radar is decided by specified low-power radio station standard of the millimeter wave in Japan [4]. We can utilize following frequency bands and bandwidth: 24GHz band (200MHz), 60GHz band (500MHz), 76GHz band (500MHz in 76-77GHz), and 79GHz band (3Gz).

FMCW (Frequency Modulation Continuous Wave) radar, which provides a high range resolution with relatively low computation load, is generally employed for current automotive radar system. However, the miss-pairing of the detected beat-frequency in the up sweep and the down sweep of FMCW tend to cause a problem under the multiple target situations in principle [5].

Authors have been developing the stepped multiple frequency Complementary Phase Code (CPC) radar [6] [7]. The unique radar modulation/demodulation method can achieve a high range resolution and a long-range detection performance by a narrow receiver bandwidth compared to total transmitting bandwidth. This scheme also accomplishes the extremely low range side lobe. Authors are developing the radar systems adopting the modulation in both 60GHz and 76GHz band.

To mitigating multipath fading problem, non-coherent integration processing, in which the received signal amplitude is averaged, is generally considered to suppress the variance of noise. Meanwhile coherent integration for signal components is considered to be effective to improve SNR [8]. Maximal Ratio Combining (MRC) that coherently integrates the signals of separated frequency bands has been suggested [3]. In this paper, at first we investigate on the multipath fading characteristics at 60GHz, 76GHz bands in the situation where the transmitting and receiving antennas are mounted at the same height of 0.4m for the point target at the altitude of 0.8 m. Then we consider several ways to employ MRC processing in stepped multiple frequency CPC.

Fig.1 Self-driving car (Robot Car) developed by the research group of the University of Electro-Communications (UEC) supported by Research and Development for Expansion of Radio Wave Resources of Ministry of Internal Affairs and Communications (MIC)

The simulation results of multipath fading environments for automotive radar are also shown.

2. Multipath Fading of automotive radar

2.1 Phase difference between direct and multipath waves

Fig.2 shows the paths of transmission and reflection waves. In this article, the multipath wave is assumed to be generated by the reflection on the road surface only. H_a is the height of the transmitting and receiving antennas. H_t is the height of the point target. The range from the receiving antenna to the target, the distance from the receiving antenna to the reflection point on the road surface, and the distance from the reflection point on the road surface to the target are R, R_1 and R_2, respectively. The elevation angle from the target to the receiving antenna is θ_d and the elevation angle from the reflection point to the receiving antenna is θ_r.

The grazing angle that is the angle between the propagating direction of the transmitting wave from transmitting antenna and the road surface is ψ ($\psi=\theta_r$). The path difference between the direct wave and multipath wave for one way is given by $dR=R_1+R_2-R$. On the other hand, the Fresnel reflection coefficients of the horizontally and vertically polarized wave Γ_h and Γ_v are given by (1) and (2), respectively.

$$\Gamma h = \frac{\sin(\psi) - \sqrt{\varepsilon_c - \cos(\psi)^2}}{\sin(\psi) + \sqrt{\varepsilon_c - \cos(\psi)^2}} \tag{1}$$

$$\Gamma v = \frac{\varepsilon_c \cdot \sin(\psi) - \sqrt{\varepsilon_c - \cos(\psi)^2}}{\varepsilon_c \cdot \sin(\psi) + \sqrt{\varepsilon_c - \cos(\psi)^2}} \tag{2}$$

Here, ε_c is a complex dielectric constant of asphalt. Specular reflection coefficient of reflection on the road surface ρs is given by (3).

$$\rho s = \exp\left(-2\left(\frac{2\pi\sigma_h \sin(\psi)}{\lambda}\right)^2\right) \tag{3}$$

where σ_h is the standard deviation of the altitude of the road surface representing the asperity of the road surfaces. The reflection coefficient ρsc of the reflection on the road surface of a multipath wave at a given point is expressed by (4) using the specular reflection coefficient ρs and Fresnel reflection coefficient Γ.

$$\rho sc = \sqrt{\mathrm{Re}(\Gamma)^2 + \mathrm{Im}(\Gamma)^2} \cdot \rho s \tag{4}$$

The phase difference between a direct wave and a multipath wave φs is described by (5) by considering the phase shift that is given by the argument of the Fresnel reflection coefficient Γ and the path difference dR.

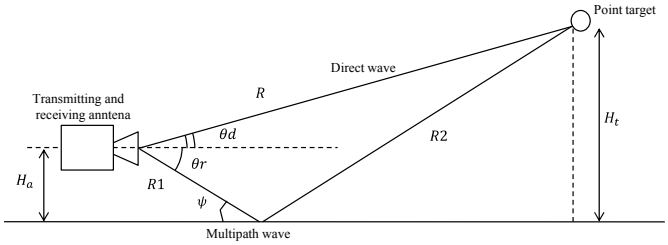

Fig.2 Illustration of the paths of the direct wave and multipath wave

$$\phi s = \arg(\Gamma) \cdot 1 + \frac{2\pi f}{c} dR \tag{5}$$

2.2 Received signal

The received signal mode vectors of the direct wave from the target to the receiving antenna Ac and multipath wave from the target to the receiving antenna Ar are described by (6) and (7), respectively.

$$Ac = \exp\left(-j\frac{2\pi f}{c}R\right) \tag{6}$$

$$Ar = \rho sc \cdot \exp\left(-j\frac{2\pi f}{c}R + \phi s\right) \tag{7}$$

It can be assumed that the propagation characteristics from the target to the receiving antenna and from the transmitting antenna to the target are the same, when the transmitting steering direction is not considered. Thus the signal mode vector of the direct wave from the transmitting antenna to the target Acc and that of the multipath wave from the transmitting antenna to the target Arc are equivalent to be Ac and Ar, respectively. As shown in Fig.2, there are 4 propagation paths from transmitting antenna to receiving antenna via the target for the round trip. The receiving signal vector is described as the summation of the signal of the 4 paths as follows.

$$Xt = Acc \cdot Ac + Acc \cdot Ar + Arc \cdot Ac + Arc \cdot Ar \tag{8}$$

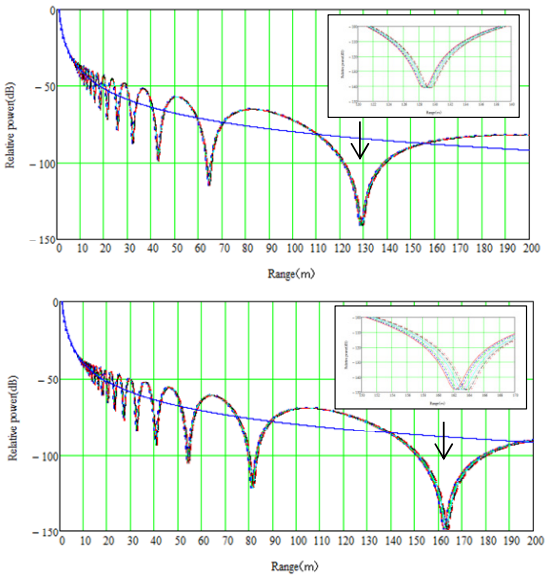

Fig.3 The receiving signal power at the target range from 1m to 200m in the multipath environment ((a) 60GHz, (b)76GHz).

2.3 Multipath fading characteristics

Fig.3 shows the received signal power at the target range from 1m to 200m in the multipath environment described in section 1 ((a) 60GHz, (b)76GHz). Here H_a and H_t are 0.4m and 0.8m, respectively. In Fig.3, the differences of the signal power of in-band are also shown. We can identify the range where the receiving signals are weakened by multipath fading at each frequency band. The ranges where the receiving signals are especially affected by multipath fading are 65m and 130m in 60GHz.There are also null points at the range of 80m and 160m in 76GHz. The width of the range where the receiving signal is weakened by multipath fading is 10-30m for each null point. The difference of receiving power (5dB-15dB) in in-band is also identified around the null points indicated by arrows as shown in Fig.3

3. Methods

3.1 Multiple Frequency Step CPC

Stepped multiple frequency CPC modulation is a hybrid method of pulse compression and synthetic bandwidth [5] [9]. In addition, this method adopts CPC pulses for the pulse compression [10]. As shown in Fig.4, the two pulses which satisfy the complementary condition are coded on the same carrier frequency. The transmitted carrier frequencies are changed N times step-like in a sequence. The same sequences are repeated M times. Fig.4 shows the block diagram of the signal processing of stepped multiple frequency CPC demodulation [6]. As shown in Fig.5, Stepped multiple frequency CPC demodulation processing is composed of following steps. After Pulse compression, Doppler frequencies, which correspond to the relative velocities of targets, are estimated by FFT associated with m on the same range bin that is equivalent to the Pulse Doppler Filter (PDF) of pulse Doppler radar. The CPC pulse compression that is the combination of Pulse compression, Compensation of Doppler shift and ADD process provides the range gate for the subsequent Synthetic Bandwidth with the extremely low range side-lobe. Finally, Synthetic bandwidth produces a high range resolution equivalent to the transmission bandwidth by a narrow band receiver compared with the transmission bandwidth. The series of coherent processing from Pulse compression to Synthetic bandwidth is expected to lead to significant SNR improvement [11]. Authors have been developing the stepped multiple frequency CPC radars operating in 60GHz and 76GHz bands. We have previously reported that the expected performance on the sidelobe and the range resolution were demonstrated by the prototype radar operated in 60GHz band [12].

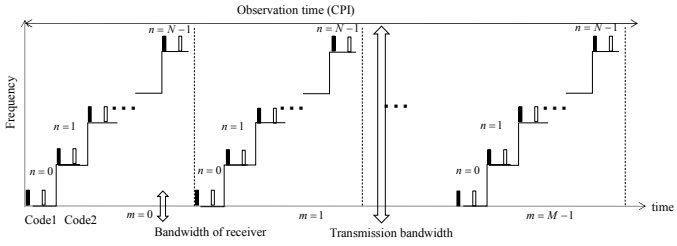

Fig.4 The transmitting sequence of stepped multiple frequency CPC

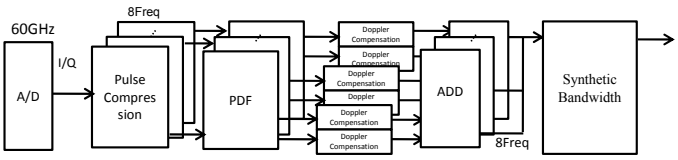

Fig.5 Schematic diagram of signal processing of stepped multiple frequency CPC

3.2 Maximal Ratio Combining (MRC) Processing in Multiple Frequency Step CPC

The synthetic bandwidth enables us to achieve a high range resolution using the information associated with the frequencies (frequency steps). Taking the multipath fading described in introduction into consideration, the robustness to multipath fading is rather important than the range resolution especially in far range for the application of Collision Avoidance etc. In this section, we consider several ways to use information associated with the frequencies for the multipath fading instead of the synthetic bandwidth in the stepped multiple frequency CPC for operating in the developed/developing 60GHz/76GHz radar. The radar parameters and expected performance are summarized in Tables 1 and 2. To utilize frequency diversity effect, the input of the signal processing for multipath fading are output data of ADD process, which still have information associated with frequency. The output data vector of ADD process associated at a range bin k in each frequency band f_g (g=0:60GHz, g=1:76GHz) is denoted by $\boldsymbol{x}_{k,g}$.

$$\boldsymbol{x}_{k,g} = \begin{pmatrix} \alpha_{k,g}(0)\exp(j\Omega_{k,g}(0)) \\ \vdots \\ \alpha_{k,g}(n)\exp(j\Omega_{k,g}(n)) \\ \vdots \end{pmatrix} + \boldsymbol{n} \tag{9}$$

where $\alpha(n)$ and $\Omega(n)$ are the amplitude and phase of received signal at the step number n obtained by (8) described in section 2.1. $\boldsymbol{n}$ denotes vector of Gaussian noise. The input data matrix $\boldsymbol{X}_{k,g}$ is also denoted by (10), where s is snapshot.

$$\boldsymbol{X}_{k,g} = (\boldsymbol{x}_{k,g}(0), \boldsymbol{x}_{k,g}(1)\ \boldsymbol{x}_{k,g}(s)\ \ldots\ \boldsymbol{x}_{k,g}(S-1)) \tag{10}$$

Fig.6 shows 4 candidates of signal processing diagram for multipath fading in using stepped multiple frequency CPC.

3.2.1 Non-coherent integration (NC)

Fig.6 (a) is a signal processing where conventional non-coherent integration is implemented instead of synthetic bandwidth in Multiple-frequency step CPC. The signal amplitudes on each range bin k is averaged S×2N (number of snapshot × number of frequency steps) times by non-coherent integration as described by (11).

$$NC_k = \frac{1}{2NS}\sum_{g=0}^{1}\sum_{s=0}^{S-1}\left\|\boldsymbol{x}_{k,g}(s)\right\|_1 \tag{11}$$

3.2.2 Non-coherent integration after MRC in each frequency band (MRC-NC)

Fig.6 (b) shows another candidate where non-coherent integration is used after MRC processing in each band. To obtain MRC weight vector for each band, the correlation matrix for each band is obtained by (12)

$$\boldsymbol{R}_{k,g} = \boldsymbol{X}_{k,g}\boldsymbol{X}_{k,g}^{H} \tag{12}$$

Here ^{H} represents the complex conjugate transpose of the

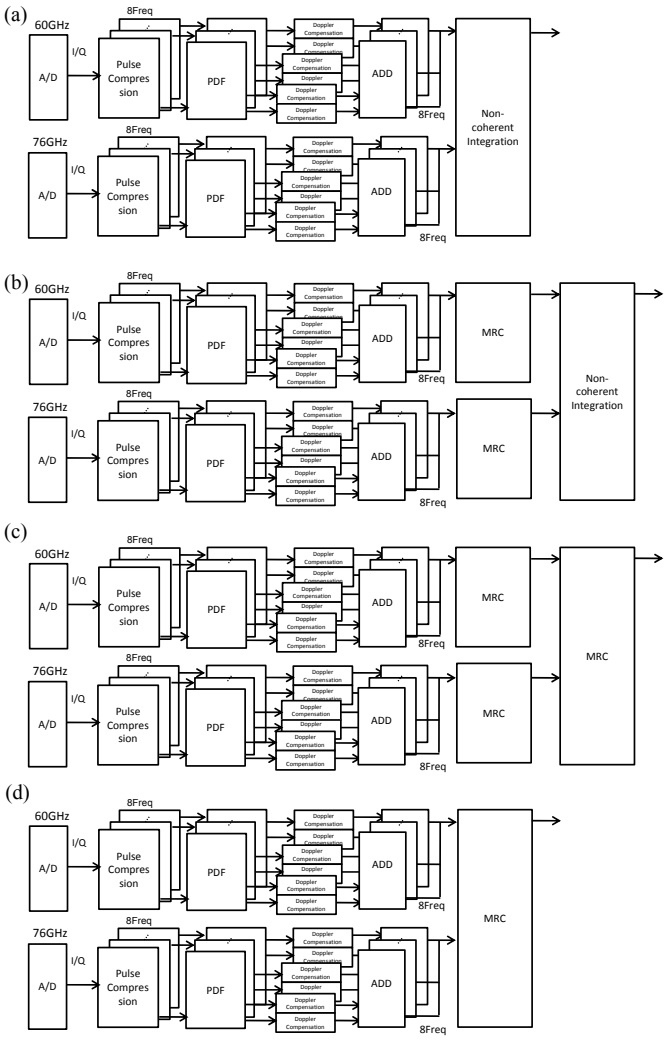

Fig.6 Four signal processing flow for multipath fading using in far range mode of multiple-frequency step CPC.

matrix. The MRC weight vectors $\boldsymbol{w}_{k,g}$ for each band and range bin are obtained by calculating the eigenvectors corresponding to the maximal eigenvalues for each band and range bin. By using $\boldsymbol{w}_{k,g}$, MRC processing for each band is performed by (13).

$$XMR_{k,g} = \frac{1}{S}\sum_{s=0}^{S-1}\left|\boldsymbol{w}_{k,g}{}^{H}\boldsymbol{x}_{k,g}(s)\right| \tag{13}$$

After MRC processing, the received signal power obtained in each band $XMR_{k,g}$ is finally integrated non-coherently over the frequency band.

$$MRNC_k = \frac{1}{2}\sum_{g=0}^{1} XMR_{k,g} \tag{14}$$

3.2.3 MRC over the frequency band after MRC in each frequency band (MRC-MRC)

Fig.6 (c) shows another candidate that employs second MRC processing over frequency bands after first MRC processing in each band. The input data Matrix $\boldsymbol{X2}_k$ of MRC over the frequency bands is obtained by using MRC weight vectors $\boldsymbol{w}_{k,g}$ in each frequency band as described by (15) and (16).

Table1. Multiple-frequency step CPC radar parameters used in the simulation

Frequency band	Sub pulse band-width (MHz)	Code Length	Δf (MHz)	Pulse repetition Interval (PRI) (us)	Number of Fre-quency steps N	Number of pulse repetitions M	Obser-vation time (CPI) (ms)	Radar ID g	f1～F8 (GHz)	Trans-mission band-width (MHz)	A/D sampling rate (MHz)
60GHz	80	16	50	2.5	8	128	5.12	0	60.32-60.67	430	160
76GHz	80	16	50	2.5	8	128	5.12	1	76.04-76.39	430	160

Table2 Expected performance of Multiple-frequency step CPC radar

Frequency band	Range Gate Width (Range bin after ADD) (m)	Range Resolution after Synthetic bandwidth (m)	Detectable maximum Velocity (Vmax)	Velocity Resolution (ΔV)
60GHz	1.87m (0.94m)	0.34m	111.6km/h	1.74 km/h
76GHz	1.87m (0.94m)	0.34m	88.8km/h	1.38km/h

$$\boldsymbol{x2}_{k,g}(s) = \boldsymbol{w}_{k,g}{}^{H}\boldsymbol{x}_{k,g}(s) \tag{15}$$

$$\boldsymbol{X2}_k = \begin{pmatrix} \boldsymbol{x2}_{k,0}(0) & \boldsymbol{x2}_{k,0}(1) & \boldsymbol{x2}_{k,0}(s) & \cdots & \boldsymbol{x2}_{k,0}(S-1) \\ \boldsymbol{x2}_{k,1}(0) & \cdots & \cdots & \cdots & \boldsymbol{x2}_{k,1}(S-1) \end{pmatrix} \tag{16}$$

After the first MRC processing, the correlation matrix for each band is calculated to obtain second MRC weight vector.

$$\boldsymbol{R2}_k = \boldsymbol{X2}_k \boldsymbol{X2}_k{}^{H} \tag{17}$$

The second MRC processing weight vectors $\boldsymbol{w2}_k$ for each range bin are obtained as the eigenvector corresponding to the maximal eigenvalue. By using $\boldsymbol{w2}_{k,g}$, the second MRC processing is performed by (18).

$$MR2_k = \frac{1}{S}\sum_{s=0}^{S-1}\left|\boldsymbol{w2}_k{}^{H}\boldsymbol{X2}_k{}^{<s>}\right| \tag{18}$$

Here $^{<>}$ represents the column vector of the matrix.

2.2.4 MRC on all frequency steps over the frequency band (MRC)

The other candidate is composed of a MRC processing using all frequency steps over the frequency bands. The input data Matrix $\boldsymbol{X3}_k$ of MRC for all frequency steps over the frequency bands is denoted by (19).

$$\boldsymbol{X3}_k = \begin{pmatrix} \boldsymbol{x}_{k,0}(0) & \boldsymbol{x}_{k,0}(1) & \boldsymbol{x}_{k,0}(s) & \cdots & \boldsymbol{x}_{k,0}(S-1) \\ \boldsymbol{x}_{k,1}(0) & \cdots & \cdots & \cdots & \boldsymbol{x}_{k,1}(S-1) \end{pmatrix} \tag{19}$$

To obtain MRC weight vector for all frequency steps over the frequency band, the correlation matrix is obtained by (20)

$$\boldsymbol{R3}_k = \boldsymbol{X3}_k \boldsymbol{X3}_k{}^{H} \tag{20}$$

The MRC weight vectors $\boldsymbol{w3}_k$ for each range bin and all frequency steps over the frequency bands are obtained by calculating the eigenvectors corresponding to large eigenvalues. By using $\boldsymbol{w3}_k$, MRC processing is performed by (21). Here, the number of significant eigenvalue is generally two, since the data vector has a discontinuity between two frequency bands as shown in section 4. Thus we employ the eigenvector corresponding to the second

largest eigenvalue as well as the eigenvector corresponding to the largest eigenvalue. The two weight vectors are denoted by ***w31*** and ***w32***, respectively.

$$MR3_k = \frac{1}{S}\sum_{s=0}^{S-1}\left| w31_k{}^H \boldsymbol{X3_k}^{<s>} + w32_k{}^H \boldsymbol{X3_k}^{<s>} \right| \quad (21)$$

3. Simulation Results

3.1 Receiving Signal

To simulate the input data matrix (10) described above, α(n) and Ω(n) are calculated for frequency steps. In this article, we show the simulation results in the situations where a single target exists at the range of 143.63m, where the multipath fading occurs in both two bands as shown in Fig.3. The targets having the relative velocity of 10km/h (2.778m/s) exist at these points at the first snapshot.

3.2 Simulation Result

Fig.7 (a) shows the range profile at the corresponding Doppler bin in 60GHz band. Fig.7 (b) also shows the range profile at the corresponding Doppler bin in 76GHz band. The arrows in Fig.7 indicate the range of 143.63m. By the multipath fading, the peaks are difficult to be identified at the range of 143.63m in the two frequency bands. Fig.8 shows the phase (argument) of the complex amplitude at the range bin of 153 (143.63m). The slopes of phase are also difficult to be identified especially in 60GHz. Except for the phase reflection at π or –π, discontinuity point is seen between two bands. Fig.9 shows eigenvalue distributions of the $\mathbf{R}_{k,0}$, $\mathbf{R}_{k,1}$, $\mathbf{R}3_k$. The panel (a) indicates the eigenvalues at range bin of 153 where the target exists in 60GHz. (b) indicates the eigenvalues at range bin where no targets exist in 60GHz.

From Fig.9, one significant eigenvalue is identified in Fig.9 (a) and (c) at the range where a target exists. On the other hand, no significant eigenvalue is identified in Fig.9 (b) and (d). In MRC-NC and MRC-MRC, eigenvectors corresponding to the maximal eigenvalues indicated by arrows in Fig.9 for two bands are calculated. In MRC-NC, the range profiles are averaged in-coherently. In MRC-MRC, second MRC process using 2 frequencies is conducted as in the same way with previous MRC process. The panel (e) indicates the eigenvalues of $\mathbf{R}3_k$ at range bin of 153 where the target exists and (f) indicates the eigenvalues at range bin where no targets exist. From Fig.9 (e), two significant eigenvalues are identified at the range where a target exists. On the other hand, no significant eigenvalue is identified in Fig.9 (f) as in the case with Fig.9 (b) and (d). That is reason why the eigenvectors corresponding to up to second largest eigenvalue are employed to obtain signal components as shown by (21). Fig.10 shows the results of 4 procedures using 16 snapshots. MRC-MRC process indicates best improvement of SNR, besides NC process indicates small dispersion value of noise compared with other methods. Fig.11 shows the noise level (a) and the standard deviation (b) related to the number of snapshots. In Fig. 11, the all peak levels of 4 methods set to be 1, which means 0 dB. NC process always takes smallest dispersion value of noise compared with other methods. MRC-MRC process indicates best improvement of SNR for all number of snapshots, although the dispersion value of noise is also highest in 4 processing candidates. However, the dispersion values

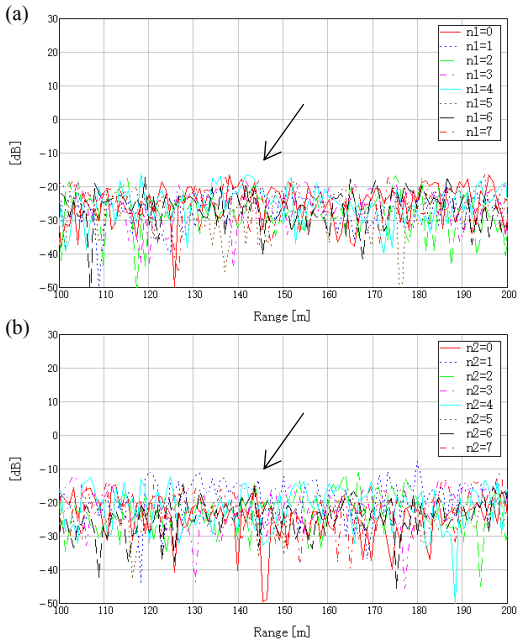

Fig.7 Range profile at the corresponding Doppler bin ((a) 60GHz, (b) 76GHz).

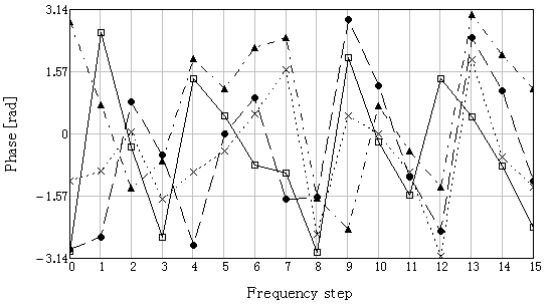

Fig.8 Phase of the complex amplitude at the peak range bin of Fig.8 (0-7:60GHz, 8-15:76GHz).

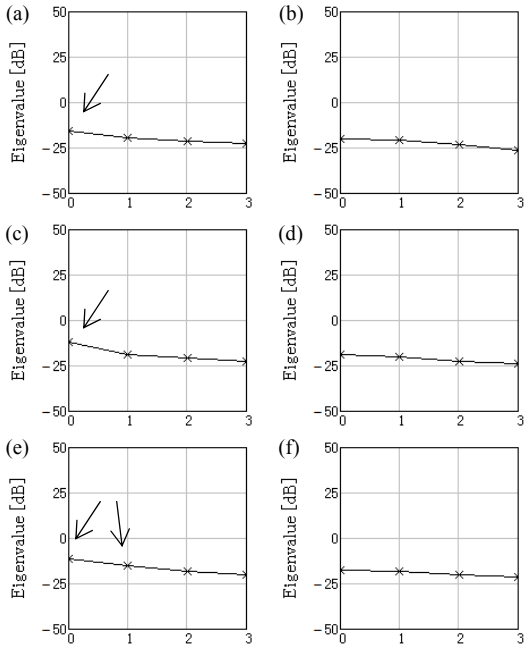

Fig.9 Eigenvalue distributions of the $\boldsymbol{R}_{k,0}$, $\boldsymbol{R}_{k,1}$, $\boldsymbol{R}3_k$ ((a) Eigenvalues of $\boldsymbol{R}_{k,0}$ (k=153), (b) Eigenvalues of $\boldsymbol{R}_{k,0}$ (k=200), (c) Eigenvalues of $\boldsymbol{R}_{k,1}$ (k=153), (d) Eigenvalues of $\boldsymbol{R}_{k,1}$ (k=200),(e) Eigenvalues of $\boldsymbol{R}_k$ (k=153), and (f) Eigenvalues of $\boldsymbol{R}_k$ (k=200)).

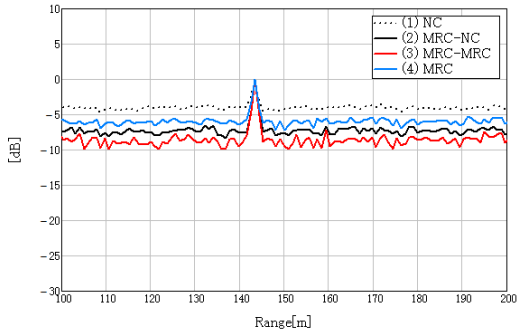

Fig.10 The output results by 4 procedures using 4 snapshots

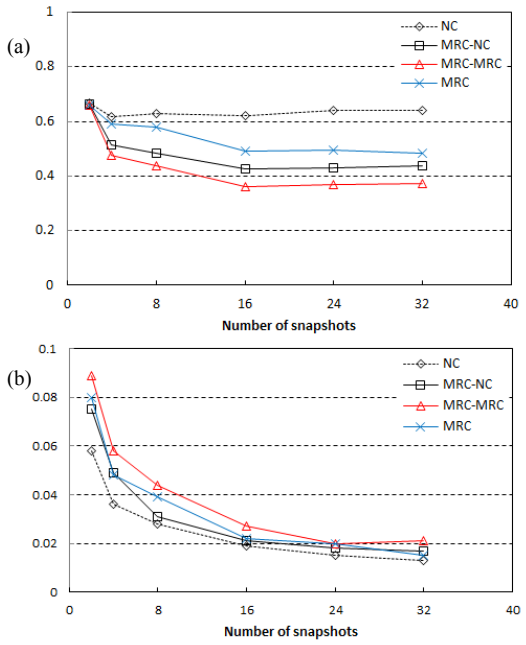

Fig.11 The output results by 4 procedures using 4 snapshots ((a) averaged noise level, and (b) standard deviation of the noise level.)

of noise of 4 processing candidates seem to be close value as the number of snapshots increase. Meanwhile we can see that the averaged noise level and the dispersion does not change very much using more than 16 snapshots. Those results indicated that the detection performance does not change very much, when the number of snapshots is 16 or larger. It is considered for a reason that the target range changes 0.46m in 32 snapshots (163.84ms), since the target has velocity. This research is an initial study on applying non-coherent integration and/or MRC to Stepped multiple frequency CPC modulation for multipath fading of automotive radar. The detection performance and false alarm rate by using 4 processing candidates using relatively small number of snapshots should be discussed in detail in the next step.

4. Conclusions

Authors have been developing stepped multiple frequency CPC radar system in consideration of applications to ITS field. The unique radar modulation and demodulation method can achieve high range resolution and long-range detection performance by a narrow receiver bandwidth compared to transmitting bandwidth. For mitigating multipath fading of automotive radar, applications of NC and MRC processing to the stepped multiple frequency CPC radar operating 60GHz and 76GHz band is considered in this paper. The conventional NC processing indicated small dispersion value of noise compared with other methods, although the method produced low SNR. MRC-MRC process indicates best improvement of SNR. This research is the initial study. The detection performance and false alarm rate by using 4 processing candidates described above should be discussed in the next step.

Acknowledgement

This research was supported by Research and Development for Expansion of Radio Wave Resources of Ministry of Internal Affairs and Communications (MIC).

Reference

[1] Y. Karasawa, “Multipath Fading Due to Road Surface Reflection and Fading Reduction by Means of Space Diversity in ITS Vehicle-to-Vehicle Communications at 60 GHz”, 2002, Electronics and Communications in Japan Part I, Vol.85, No.1, pp.35-42.

[2] H. Wang, Y. Huang, and S. Chung, “Spatial-Diversity 24-GHz FMCW Radar With Ground Effect Compensation for Automotive Application”, 2016, IEEE Transactions on Vehicular Technology, Vol.99, pp. 1–10.

[3] T. Inaba, and K. Araki, “Space-Frequence Maximal Ratio Combining for Low-Elevation Radar Target”, 2004, Electronics and Communications in Japan, Part I, Vol.87, No.5, pp.75-85.

[4] Association of Radio Industries and Businesses (ARIB), “ARIB STD-T73 ver.1.2”, 2012

[5] M. I.Skolnik, “Introduction to Radar Systems”, 1962, McGraw-Hill, New York, pp.81-92.

[6] M. Watanabe, T. Inaba, H. Thubota, T. Yano, “Development of Millimeter wave Radar uing Stepped Multiple Frequency Complementary Phase Code Modulation”, IEICE Technical Report SANE2011-81, pp.99-104, 2011.

[7] M. Watanabe and T. Inaba, “Evaluation of Millimeter wave Radar uing Stepped Multiple Frequency Complementary Phase Code Modulation”, IEICE Technical Report SANE2012-68, pp.67-72, 2012

[8] J. I. Marcum, “Statistical Theory of Target Detection, Mathematical Appendix”, 1960, IRE Trans. On IT, vol. IT-6, No.2.

[9] N. Levanon, "Stepped-Frequency Pulse-Train Radar Signal", 2002, Radar, Sonar and Navigation, IEE Proceedings, vol.149, No.6, pp.198-309.

[10] C. Gonzales, R. Woodman, “Pulse compression techniques with application to HF probing of the mesosphere”, Radio Science, Volume 19, Number 3, Pages 871-877, 1984

[11] M. Akita, Y. Ota, M. Watanabe, T. Inaba, “Experimental Verification for Detectable Range Performance of Stepped Multiple Frequency CPC and Pulse Compression”, IEICE Technical Report SANE2016-49, pp.51-56, 2016 (in Japanese).

[12] M. Watanabe, M. Akita, and T. Inaba, Stepped Multiple Frequency Complementary Phase Code Radar and the Fundamental Experiment, 2015, IEEJ Transactions on Electronics, Information and Systems Vol. 135, No.3, pp. 285-291 (in Japanese).